SCIENTIFIC REPORTS

OPEN

Spin-Selective Transmission and Devisable Chirality in Two-Layer Metasurfaces

Received: 19 May 2017
Accepted: 10 July 2017
Published online: 15 August 2017

Zhancheng Li, Wenwei Liu, Hua Cheng, Shuqi Chen & Jianguo Tian

Chirality is a nearly ubiquitous natural phenomenon. Its minute presence in most naturally occurring materials makes it incredibly difficult to detect. Recent advances in metasurfaces indicate that they exhibit devisable chirality in novel forms; this finding offers an effective opening for studying chirality and its features in such nanostructures. These metasurfaces display vast possibilities for highly sensitive chirality discrimination in biological and chemical systems. Here, we show that two-layer metasurfaces based on twisted nanorods can generate giant spin-selective transmission and support engineered chirality in the near-infrared region. Two designed metasurfaces with opposite spin-selective transmission are proposed for treatment as enantiomers and can be used widely for spin selection and enhanced chiral sensing. Specifically, we demonstrate that the chirality in these proposed metasurfaces can be adjusted effectively by simply changing the orientation angle between the twisted nanorods. Our results offer simple and straightforward rules for chirality engineering in metasurfaces and suggest intriguing possibilities for the applications of such metasurfaces in spin optics and chiral sensing.

Chirality, a signature aspect of materials in the organic world, is defined as the quality of objects that lack mirror-image symmetry in three-dimensional space[1,2]. Chirality exists in a wide array of naturally occurring molecules, such as carbohydrates, amino acids, and proteins. Thus, chirality attracts the attention of researchers investigating the fundamentals of both biology and chemistry[1–4]. Contemporary research defines circular dichroism (CD) spectra as the difference in absorbance for left-handed circular-polarized (LCP) and right-handed circular-polarized (RCP) waves; CD spectra serve as the main means for chirality detection and discrimination. LCP and RCP waves have opposite spin and appear in processes that display inherent chirality[5]. Consequently, circular-polarized waves with opposite spins (LCP or RCP) interact differently with chiral materials[6]. However, the chirality of natural molecules is quite subtle, and its detection and discrimination are difficult.

Over the past decade, advances in metamaterials and metasurfaces have provided extensive opportunities for developments in chirality studies and sensing[6–10]. Compared to naturally occurring molecules, these artificial nanostructures show significantly enhanced chiral optical responses that are crucial to the understanding of chirality and provide an effective way to improve conformational and structural analyses in both biology and chemistry[11–13]. Recently, chirality in three-dimensional space leading to CD has gathered significant scientific interest, as has two-dimensional chirality and extrinsic chirality[14–17]. Previous research projects investigating chiral optical responses of artificial nanostructures have sparked the development of chiral nanophotonics.

In contemporary research, chiral artificial nanostructures have played important roles in spin optics and polarization controlling because of their polarization-selective responses. Rodrigues *et al.* demonstrated a spin-selective enhancement of two-photon luminescence from quantum emitters based on a chiral-arc metamaterial[18]. Wang *et al.* demonstrated spin-selective metamirrors that enable selective, near-perfect reflection of designated circularly polarized waves without reversing their handedness and provide complete absorption of the other polarization states[19]. In addition, Kenney *et al.* demonstrated a Pancharatnam–Berry phase-induced spin-selective transmission in herringbone-dielectric metamaterials[20]. These demonstrated artificial nanostructures provide revolutionary insights into spin-selective interactions between optical systems and electromagnetic waves and offer wide-ranging possibilities for nanophotonics applications. Thus, providing simple and straightforward rules for designing and engineering chiral optical responses of artificial nanostructures is important. An effective approach to selecting the spin of transmission-mode incident waves without polarization conversion

The Key Laboratory of Weak Light Nonlinear Photonics, Ministry of Education, School of Physics and TEDA Institute of Applied Physics, Nankai University, Tianjin, 300071, China. Correspondence and requests for materials should be addressed to S.C. (email: schen@nankai.edu.cn)

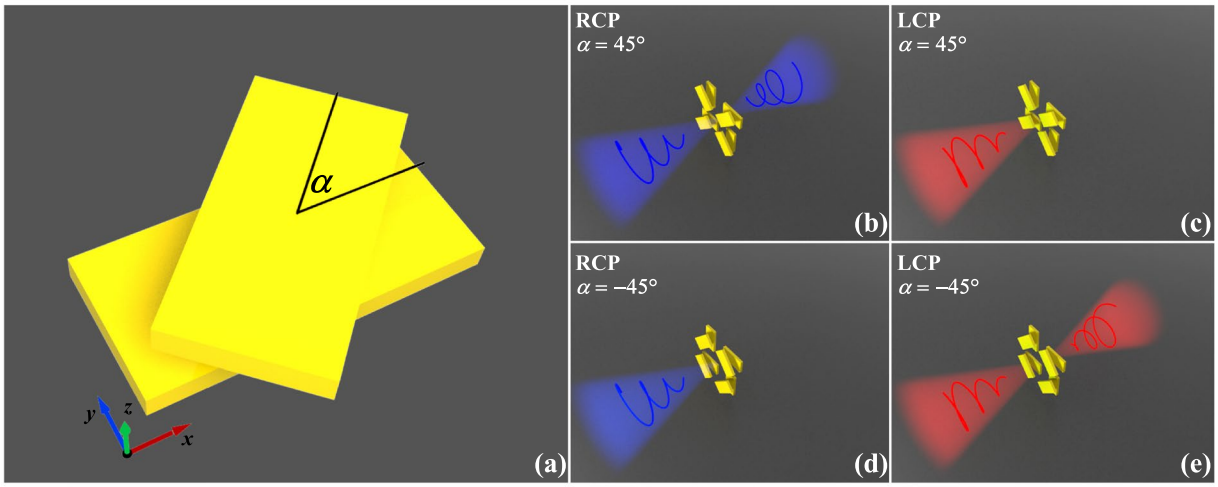

Figure 1. Design schematic for two-layer metasurfaces based on twisted nanorods. (**a**) The schematic of a twisted nanorod structure with orientation angle α. The designed two-layer metasurfaces, which are C_4-symmetric, consist of four rotationally twisted nanorod structures with the same orientation angle. (**b**) to (**e**) Illustrations of spin-selective transmission in the two-layer metasurfaces for twisted nanorods with orientation angle α equal to 45° or −45°. The chiral optical responses exhibited by these two metasurfaces are opposite; thus, they can be treated as enantiomers.

also is desirable. Moreover, achieving a simple means for the continuous engineering of chiral optical responses of artificial nanostructures plays an irreplaceable role in applications employing spin optics and chiral sensing.

Here, we propose using two-layer metasurfaces based on twisted nanorods to generate spin-selective transmissions and to achieve chirality engineering in the near-infrared region. The proposed metasurfaces exhibit C_4-symmetry relative to the wave-transmission direction but lack any additional reflection symmetry. This design is based on the theoretical predictions using advanced Jones calculus analysis and then demonstrated using simulations. We designed two metasurfaces with opposite spin-selective transmission at 1650 nm with over 50% efficiency. These metasurfaces can be treated as enantiomers and used as spin selectors between 1640 nm to 1652 nm. Moreover, we demonstrate that the chirality of the proposed metasurfaces can be engineered easily by simply changing the orientation angle of the twisted nanorods.

Theoretical Analysis. Materials can be classified based on their structural symmetry. Here, advanced Jones calculus is used to analyze the chirality and theoretical conditions of spin-selective transmission in periodic metasurfaces[21]. The complex amplitudes of circularly polarized incident and transmitted fields can be related by the complex Jones matrix **T**, where

$$\begin{pmatrix} t_{\mathrm{LCP}} \\ t_{\mathrm{RCP}} \end{pmatrix} = \begin{pmatrix} t_{\mathrm{LL}} & t_{\mathrm{LR}} \\ t_{\mathrm{RL}} & t_{\mathrm{RR}} \end{pmatrix} \begin{pmatrix} i_{\mathrm{LCP}} \\ i_{\mathrm{RCP}} \end{pmatrix} = \mathbf{T}_{\mathrm{circ}} \begin{pmatrix} i_{\mathrm{LCP}} \\ i_{\mathrm{RCP}} \end{pmatrix}. \tag{1}$$

Here, the subscript "circ" of $\mathbf{T}_{\mathrm{circ}}$ indicates that the Jones matrix lies in the circular base.

CD spectra always can characterize the chirality of structures. For structures with C_4-symmetry respect to the z axis, the difference of the transmission intensity ΔT for RCP and LCP illumination is directly correlated to CD, so that

$$\Delta T = T_{\mathrm{LCP}} - T_{\mathrm{RCP}}, \tag{2}$$

where $T_i = |t_i|^2$ is the squared moduli of the transmitted electric field.

For the structures with C_4-symmetry relative to the z axis but without any additional reflection symmetry, The **T** matrix in the linear base is

$$\mathbf{T}_{\mathrm{lin}} = \begin{pmatrix} t_{xx} & t_{xy} \\ -t_{xy} & t_{xx} \end{pmatrix}, \tag{3}$$

the $\mathbf{T}_{\mathrm{circ}}$ can then be obtained by a change of the base vectors[21,22]

$$\mathbf{T}_{\mathrm{circ}} = \begin{pmatrix} t_{\mathrm{LL}} & t_{\mathrm{LR}} \\ t_{\mathrm{RL}} & t_{\mathrm{RR}} \end{pmatrix} = \frac{1}{2} \begin{pmatrix} t_{xx} + t_{yy} + i\left(t_{xy} - t_{yx}\right) & t_{xx} - t_{yy} - i\left(t_{xy} + t_{yx}\right) \\ t_{xx} - t_{yy} + i\left(t_{xy} + t_{yx}\right) & t_{xx} + t_{yy} - i\left(t_{xy} - t_{yx}\right) \end{pmatrix}, \tag{4}$$

then, the **T** matrix in the circular base is

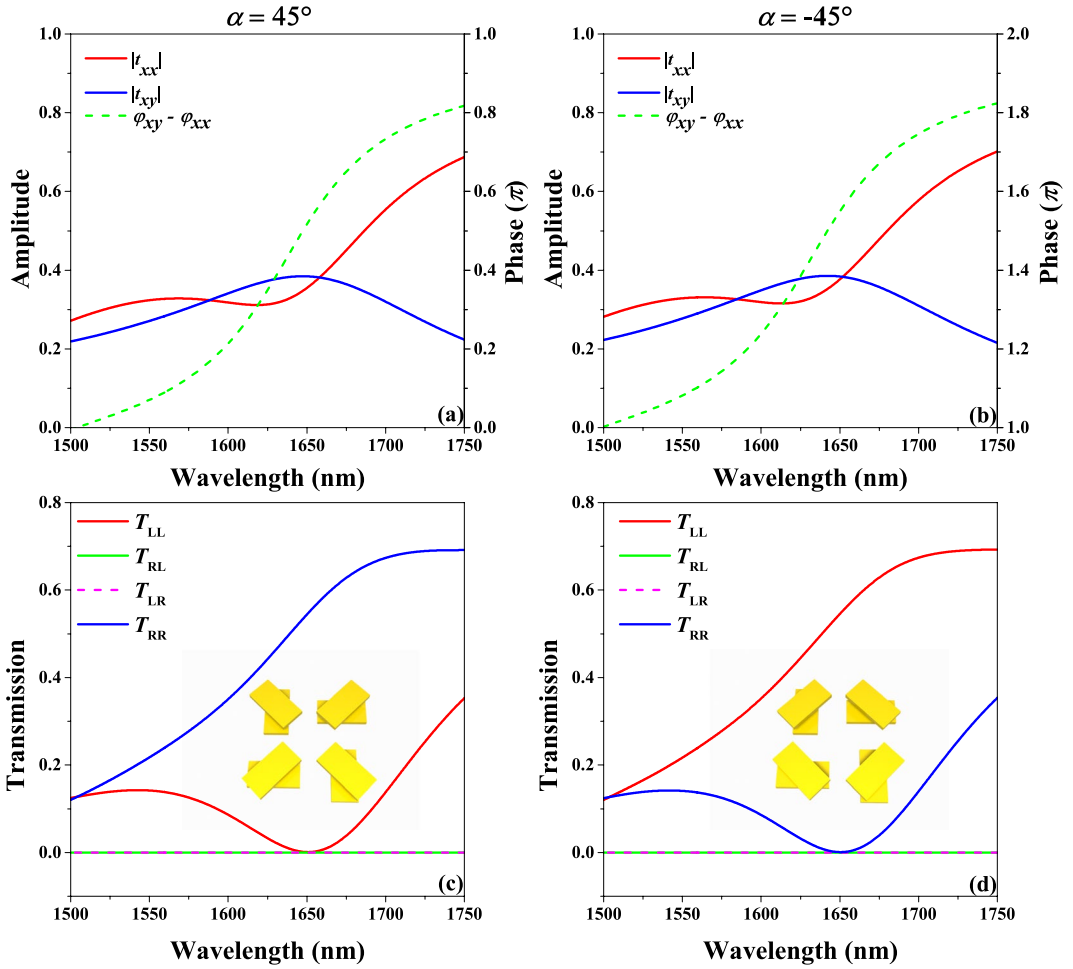

Figure 2. The analysis of **T** matrix coefficients of the designed metasurface. (**a**) and (**b**) Simulation results of the amplitudes and phase differences of linear base coefficients t_{xx} and t_{xy} of the two-layer metasurface with values of the orientation angle α of 45° and −45°, respectively. (**c**) and (**d**) Simulation results for the squared moduli $T_{ij} = |t_{ij}|^2$ of the circular base coefficients of the two-layer metasurface with values of the orientation angle α of 45° and −45°, respectively.

$$\mathbf{T}_{\text{circ}} = \begin{pmatrix} t_{\text{LL}} & 0 \\ 0 & t_{\text{RR}} \end{pmatrix} = \begin{pmatrix} t_{xx} + it_{xy} & 0 \\ 0 & t_{xx} - it_{xy} \end{pmatrix}. \tag{5}$$

The difference of the transmission intensity ΔT is then given by

$$\Delta T = T_{\text{LCP}} - T_{\text{RCP}} = -4|t_{xx}| \cdot |t_{xy}| \cdot \sin(\varphi_{xy} - \varphi_{xx}), \tag{6}$$

where φ_{ij} is the phase of the complex coefficients t_{ij}. Thus, the chirality of this kind of structure is determined by the amplitude and phase difference of the linear-based complex coefficients t_{xx} and t_{xy}.

Either t_{LL} or t_{RR} must be zero for a spin-selective transmission to be generated. Thus, the amplitudes of complex coefficients t_{xx} and t_{xy} must be equal while their phases must show a difference of $-\pi/2$ or $\pi/2$. When the phase difference between t_{xx} and t_{xy} is $-\pi/2$, only LCP incidence can be transmitted without polarization conversion. Likewise, when the phase difference between t_{xx} and t_{xy} is $\pi/2$, only RCP incidence can be transmitted without polarization conversion.

Hence, spin-selective transmission can be obtained when the above-mentioned condition is satisfied. Furthermore, the chirality of structures with C_4-symmetry relative to the z axis but with no additional reflection symmetry can be engineered by designing the complex coefficients t_{xx} and t_{xy} to be reasonable.

Results and Discussion

We used the twisted gold nanorod structure shown in Fig. 1a to satisfy the above-mentioned conditions and achieve spin-selective transmission. The nanorods had length l of 300 nm, width w of 120 nm, and thickness t of 30 nm. The layer-to-layer separation distance d was 40 nm. The orientation angle α indicated the relative rotation angle between the top and bottom nanorods. The designed two-layer metasurfaces consisted of four rotationally

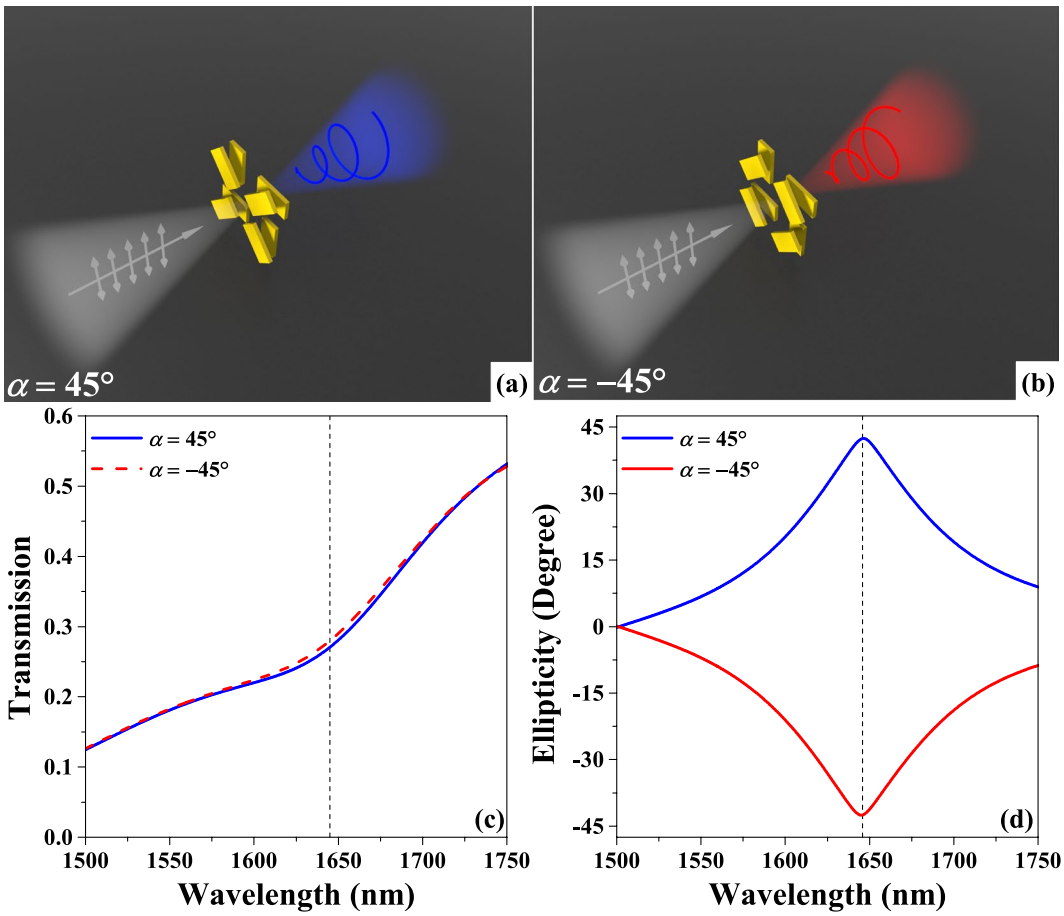

Figure 3. The performance of the designed metasurface as a spin selector. (**a**) and (**b**) Illustrations of the spin selection of the proposed two-layer metasurface with values of the orientation angle α of 45° and −45°, respectively. (**c**) and (**d**) Simulation results for transmission intensity and ellipticity when the incidence is *y*-polarized.

twisted nanorod structures with the same orientation angle. Each designed metasurface had a unit-cell period P of 700 nm in both the x and y directions. The proposed metasurfaces were embedded in a SiO_2 substrate to prevent wave interference at the interface of the air and substrate. The thickness d_2 of the SiO_2 covering on the top nanorods was 270 nm. This design can be fabricated on a SiO_2 substrate with a mature layer-by-layer fabrication process[12,23]. The designed metasurfaces display C_4-symmetry relative to the z axis but with no additional reflection symmetry when the orientation angle α was not either 0° or 90°. Figure 1b,d show two different designs with orientation angle α equal to 45° and −45°, respectively.

First, we simulate and discuss the **T** matrix coefficients of the designed metasurface with spin-selective transmission. Figure 2a,b show the amplitude and phase differences of linear base coefficients t_{xx} and t_{xy} for the two designed metasurfaces with orientation angle α of 45° and −45°, respectively. The metasurface with orientation angle α of 45° shows a phase difference between coefficients t_{xx} and t_{xy} close to $\pi/2$ around 1650 nm while the amplitudes of t_{xx} and t_{xy} are nearly equal. The metasurface with orientation angle α of −45° displays a phase difference between coefficients t_{xx} and t_{xy} close to $-\pi/2$ around 1650 nm while the amplitudes of t_{xx} and t_{xy} are nearly equal. The amplitude and phase difference of t_{xx} and t_{xy} of the proposed metasurfaces with orientation angles α of 45° and −45°, respectively, approximately fit the abovementioned conditions, which indicates the existence of spin-selective transmission in these metasurfaces around 1650 nm. The squared moduli $T_{ij} = |t_{ij}|^2$ of the circular base coefficients are simulated and shown in Fig. 2c,d for the designed metasurfaces with orientation angles α of 45° and −45°, respectively. The results show that for the metasurface with an orientation angle α of 45°, only T_{RR} does not equal to zero at 1650 nm, which means that only an RCP incident wave can be transmitted. In contrast, for the metasurface with an orientation angle α of −45°, only an LCP incident wave can be transmitted at 1650 nm, as shown in Fig. 1b to e. The transmission efficiency is over 50% around 1650 nm. Without SiO_2 covering layer, the working wavelength of the spin-selective transmission will blue shift and its performance will reduce.

The spin-selective transmission in the designed metasurface is attributed to its chirality without any polarization conversion effect. Thus, these metasurfaces can be used for spin selection. The performance of the designed metasurface as a spin selector is shown in Fig. 3. Here, Fig. 3a,b provide illustrations of the spin selection in the designed metasurfaces. Arbitrarily polarized incident waves can be decomposed into LCP and RCP components. Only the LCP or RCP components of such incident waves can be transmitted in the designed metasurfaces with

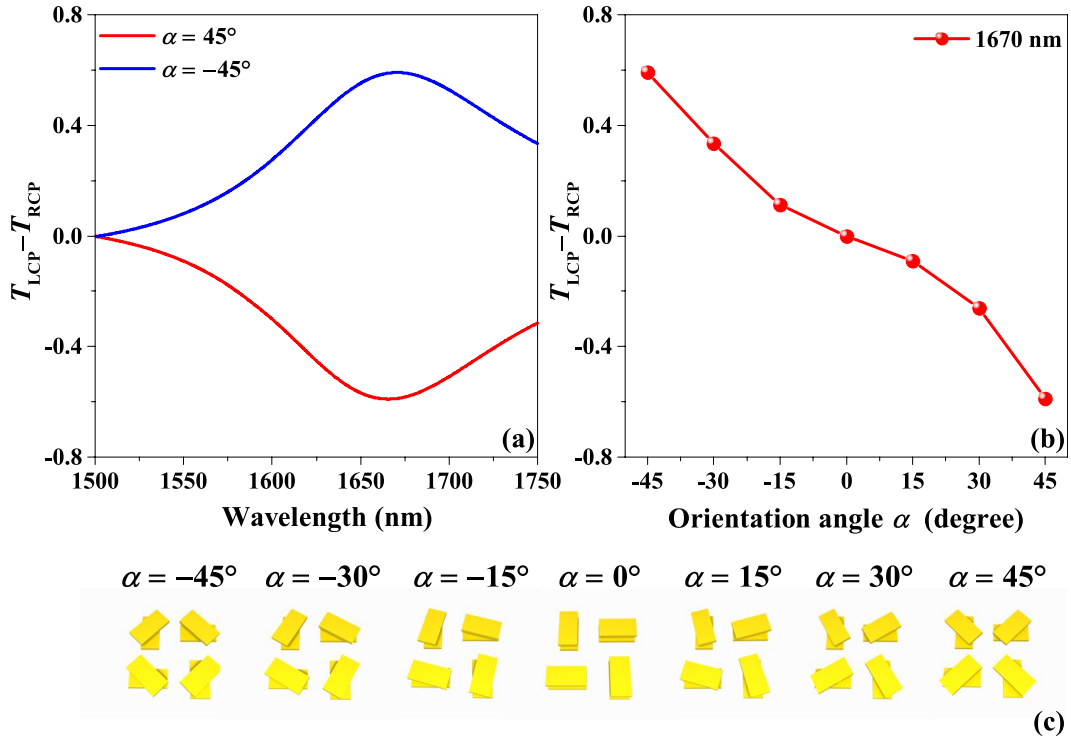

Figure 4. Characterizations of the chirality of the designed metasurfaces. (**a**) Simulation results for transmission difference $\Delta T = T_{LCP} - T_{RCP}$ of the two-layer metasurface with values of the orientation angle α of 45° and −45°, respectively. (**b**) Engineering of the transmission difference by orientation angle. (**c**) Schematic diagrams of various two-layer metasurfaces with different orientation angles in 15° increments from −45° to 45°.

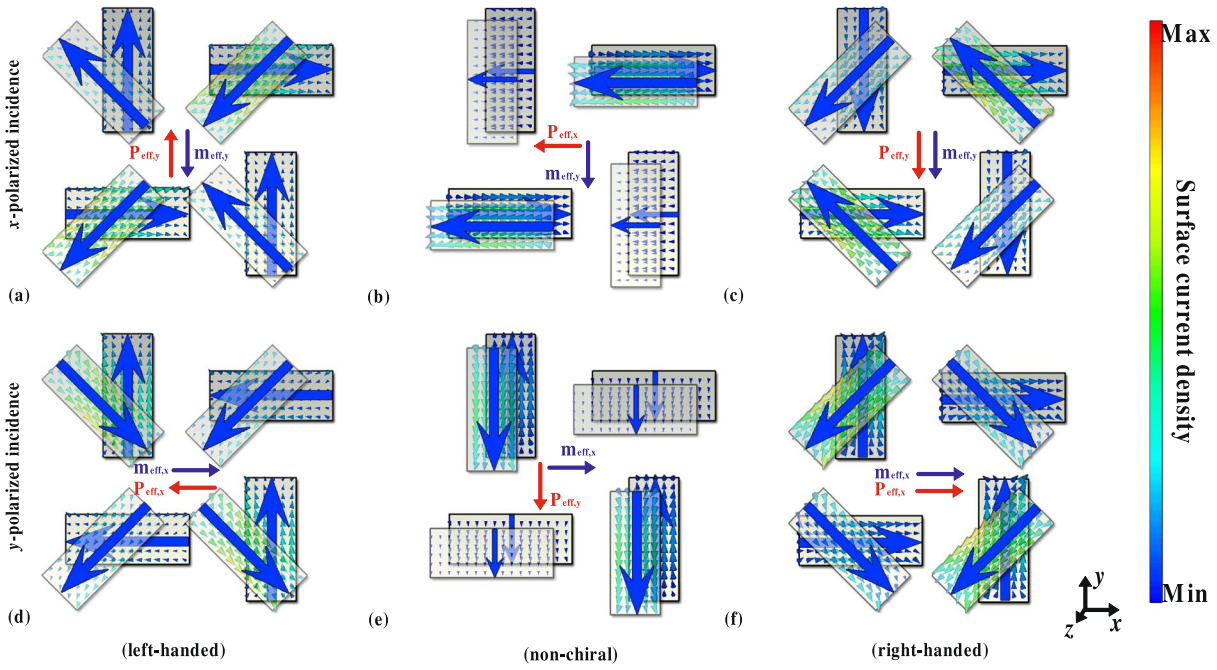

Figure 5. Simulated surface current distributions of the two-layer metasurfaces at 1670 nm. The surface current density for designed two-layer metasurfaces with orientation angle equal to (**a**) (**d**) 45°, (**b**) (**e**) 0° and (**c**) (**f**) −45°, respectively with (**a**–**c**) *x*-polarized and (**d**–**f**) *y*-polarized incidence. The induced electric and magnetic dipoles have antiparallel components and parallel components for orientation angle equal to 45° and −45° respectively, resulting in the opposite handedness of the two-layer metasurfaces.

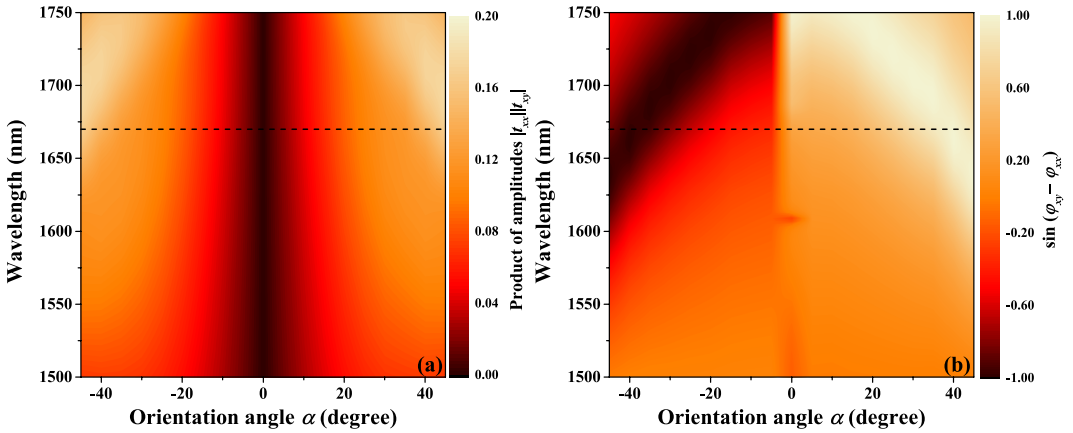

Figure 6. The relationship between the chiral response of the designed metasurface and its orientation angle. Simulation results for two-layer metasurfaces with different orientation angles and wavelengths. (**a**) Products of amplitudes $|t_{xx}|\cdot|t_{xy}|$ for the linear base transmission coefficients t_{xx} and t_{xy}. (**b**) Sine value of phase difference $\varphi_{xy}-\varphi_{xx}$.

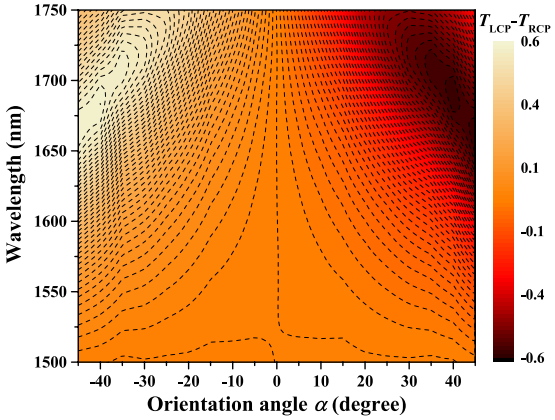

Figure 7. Simulation results for the transmission difference $\Delta T = T_{\mathrm{LCP}} - T_{\mathrm{RCP}}$ of two-layer metasurfaces with different orientation angles and wavelengths. The black dashed lines indicate the boundaries of different values of ΔT.

orientation angles α of −45° or 45°, respectively. When incidence is *y*-polarized, the transmission intensities are nearly equal across the examined waveband from 1500 nm to 1750 nm for those two metasurfaces. At the same time, their ellipticities have the same amplitudes but with opposite signs, as shown in Fig. 3c,d. The ellipticity of waves is defined as $\phi = \frac{1}{2}\arcsin\left(\frac{2r}{1+r^2}\sin\Delta\varphi\right)$, where r represents the amplitude ratio given by $r = |t_y|/|t_x|$ and $\Delta\varphi$ represents the phase difference between t_x and t_y, given by $\Delta\varphi = \varphi_y - \varphi_x$, thus indicating the shape of the polarization ellipse. The ellipticity of the transmitted wave equals zero, meaning that the transmitted wave is ideally linearly polarized. When the ellipticity of the transmitted wave equals −45° or 45°, it represents LCP and RCP, respectively. The ellipticity of the transmitted wave is less than −40° from 1640 nm to 1652 nm and reaches a minimum value of −42.4° at 1646 nm in the designed metasurface with an orientation angle α of −45°. Also, the ellipticity of the transmitted wave exceeds 40° from 1640 nm to 1652 nm and reaches a maximum value of 42.4° at 1646 nm in the designed metasurface with an orientation angle α of 45°. The transmission intensity is around 28% at 1646 nm. For linear-polarized waves with arbitrary polarization directions, the amplitudes of the LCP and RCP components are in equal. Thus, the LCP and RCP components of such waves can be selected effectively by these two kinds of metasurfaces with equivalent transmission intensities around 28%, relative to the incident intensities, for wavelengths around 1646 nm.

Characterizations of the chirality of the designed metasurfaces can be obtained by simulating the transmission differences $\Delta T = T_{\mathrm{LCP}} - T_{\mathrm{RCP}}$, as Fig. 4 shows. Figure 4a depicts the transmission differences of the designed metasurfaces with orientation angles α of 45° and −45°, respectively. The amplitudes of the transmission difference exhibited by these two kinds of metasurfaces are equivalent; both reach a maximum value 0.58 at 1670 nm while their signs are opposite, which indicates their chiral optical responses are opposite. Thus, these two kinds of metasurfaces can be treated as enantiomers. Figure 4b shows the relationship between the transmission difference and orientation angle at 1670 nm, which indicates that the chirality of the metasurfaces can be engineered simply

by changing the orientation of the twisted nanorods. The symmetry of the designed metasurface changes from C_4-symmetry relative to the z axis, but with no additional reflection symmetry, to mirror symmetry perpendicular to the z axis as the orientation angle α varies from $-45°$ to 0°. In addition, the symmetry of the designed metasurface changes from the mirror symmetry perpendicular to the z axis to a C_4-symmetry relative to the z axis, but with no additional reflection symmetry, as the orientation angle α varies from 0° to 45°, as shown in Fig. 4c. These results indicate that the variation of chirality is consistent with the variation of the symmetry of the metasurface.

In our simulations, we found that the near field interference in the designed two-layer metasurfaces plays an important role for the origin and the variation of its chirality. Thus, even though the designed two-layer metasurfaces consisted of four rotationally twisted nanorod structures, the chiral response of the designed two-layer metasurfaces cannot be directly obtained from the single twisted nanorod structure by using the advanced Jones calculus[24]. To further show the origin and the variation of the chirality in designed two-layer metasurfaces, we gave the dipolar analysis for the designed two-layer metasurfaces. Similar to natural chiral molecules, the specific combination of the electric and magnetic responses along the same direction, that is, parallel or antiparallel orientations with comparable magnitude, can induce strong chiral response[25,26]. A right-handed enantiomer refers to the one whose components of effective electric and magnetic dipoles in the same direction are parallel orientation, while a left-handed enantiomer refers to the one whose components of effective electric and magnetic dipoles in the same direction are antiparallel orientation. To clarify the chiral response of the designed two-layer metasurfaces, we give the simulated surface current distribution at 1670 nm for three metasurfaces with different orientation angles for x- or y-polarized incidence in Fig. 5. It is noticeable that the direction of induced magnetic dipoles are always perpendicular to the polarization direction of the incidence and the direction of the effective electric dipoles of the top layer are always parallel to the polarization direction of the incidence. Moreover, the effective electric dipoles of the bottom layer have a component perpendicular to the polarization direction of the incidence while the orientation angle of the two-layer metasurfaces is not equal to 0°. For two-layer metasurfaces with orientation angle α of 45°, the components of its effective electric and magnetic dipoles perpendicular to the polarization direction of the incidence are antiparallel with each other, which result in a strong left-handed chiral response. There is no chiral response for two-layer metasurfaces with orientation angle α of 0° because its effective electric and magnetic dipoles have no component in the same direction. For two-layer metasurfaces with orientation angle α of $-45°$, the components of its effective electric and magnetic dipoles perpendicular to the polarization direction of the incidence are parallel with each other, which result in a strong right-handed chiral response. Moreover, with varying the orientation angle α from 45° to 0° or $-45°$ to 0°, the magnitudes of the components of the effective electric and magnetic dipoles perpendicular to the polarization direction of the incidence will decrease and increase respectively, which result in the reduction of the chiral response.

The relationship between the variation of the chiral response of the designed metasurface and its orientation angle can be intuitively elucidated by examining the product of the amplitudes $|t_{xx}|\cdot|t_{xy}|$ and the sine value of the phase difference $\varphi_{xy} - \varphi_{xx}$ of the linear-based transmission coefficients t_{xx} and t_{xy} of the designed metasurfaces with different orientation angles and wavelengths. Figure 6 illustrates a simulation of this relationship. Equation 6 indicates that the amplitude of the transmission difference is determined by the product of the amplitudes $|t_{xx}|\cdot|t_{xy}|$ and the sine value of the phase difference $\varphi_{xy} - \varphi_{xx}$ while its sign is determined by the sign of the sine value of the phase difference. The black dashed lines in Fig. 6 indicate the products of the amplitudes and sine values of the phase differences for various orientation angles at 1670 nm. The product of the amplitudes and the amplitudes of the sine value decrease at first and then increase as the orientation angle α varies from $-45°$ to 45°. Concurrently, the sign of the sine value changes from negative to positive. It is important to note that the variations of the product of amplitudes and the amplitudes of the sine values are symmetric as the orientation angle α varies from 0° to $-45°$ and 0° to 45°. These results indicate that both the amplitude and the sign of the transmission difference are devisable by simply changing the orientation angle. Thus, the chiral optical response of the designed metasurface is devisable. Moreover, this relationship exists not only at 1670 nm but also across a broad waveband, especially between 1600 nm and 1750 nm. This finding indicates that conditions for chirality engineering exist in a broad waveband. The simulation results for transmission differences of the designed metasurfaces with different orientation angles and wavelengths are shown in Fig. 7. These results confirm our prediction. Therefore, the transmission difference of the designed metasurface can be varied continuously by changing the orientation angle across a broad waveband.

Conclusion

We proposed the underlying theory, design specifications, and simulated demonstration of spin-selective transmission and chirality engineering in two-layer metasurfaces based on twisted nanorods in the near-infrared region. Using the results of the theoretical analysis employing advanced Jones calculus, we designed metasurfaces displaying C_4-symmetry relative to the wave transmission direction but with no additional reflection symmetry. This designed metasurfaces then were optimized and used to simulate spin-selective transmission and chirality engineering. The simulation results are consistent with the theoretical prediction. Two-layer metasurfaces with opposite spin-selective transmission were realized at 1650 nm with over 50% efficiency. Thus, these two two-layer metasurfaces can be treated as enantiomers. The spin-selective transmission in the designed metasurfaces is attributed to their chirality with no polarization conversion effect. Thus, these metasurfaces can be used for spin selection between 1640 nm and 1652 nm with amplitudes of ellipticity greater than 40°. Moreover, we demonstrated that the chirality of the proposed metasurfaces can be engineered easily by simply changing the orientation angle of the twisted nanorods across a broad waveband. These results offer simple and straightforward rules for chirality engineering of metasurfaces and provide helpful insights and intriguing possibilities for applications in spin optics and enhanced chiral sensing in biological and chemical applications.

Methods

Numerical simulations using the finite-differential time-domain (FDTD) method have been conducted to analyze the characterizations of the designed metasurface. Perfectly matched layers were used at the top and bottom of the simulation domain to completely absorb waves, leaving the simulation domain in the direction of propagation. Periodic boundary conditions were used in the x and y directions representing a periodical structure. The permittivity of the SiO_2 was taken as 2.25. The dispersion function of gold was defined by the Drude model with a plasma frequency ω_p of $1.37 \times 10^{16}\,s^{-1}$ and damping constant γ of $1.224 \times 10^{14}\,s^{-1}$ [27,28].

References

1. Schäferling M. *Chiral Nanophotonics*. (Switzerland, Springer International Publishing, 2017)
2. Khanikaev, A. B. *et al*. Experimental demonstration of the microscopic origin of circular dichroism in two-dimensional metamaterials. *Nat. Commun.* **7**, 12045 (2016).
3. Zhou, J. *et al*. Terahertz chiral metamaterials with giant and dynamically tunable optical activity. *Phys. Rev. B* **86**, 035448 (2012).
4. Wu, L. *et al*. Electromagnetic manifestation of chirality in layer-by-layer chiral metamaterials. *Opt. Express* **21**, 5239–5246 (2013).
5. Bliokh, K. Y., Rodríguez-Fortuño, F. J., Nori, F. & Zayats, A. V. Spin-orbit interactions of light. *Nat. Photon.* **9**, 796–808 (2015).
6. Hentschel, M., Schäferling, M., Weiss, T., Liu, N. & Giessen, H. Three-dimensional chiral plasmonic oligomers. *Nano Lett.* **12**, 2542–2547 (2012).
7. Hentschel, M., Schäferling, M., Metzger, B. & Giessen, H. Plasmonic diastereomers: adding up chiral centers. *Nano Lett.* **13**, 600–606 (2013).
8. Yin, X., Schäferling, M., Metzger, B. & Giessen, H. Interpreting chiral nanophotonic spectra: the plasmonic Born–Kuhn model. *Nano Lett.* **13**, 6238–6243 (2013).
9. Ferry, V. E., Hentschel, M. & Alivisatos, A. P. Circular dichroism in off-resonantly coupled plasmonic nanosystems. *Nano Lett.* **15**, 8336–8341 (2015).
10. Duan, X., Yue, S. & Liu, N. Understanding complex chiral plasmonics. *Nanoscale* **7**, 17237–17243 (2015).
11. Gansel, J. K. *et al*. Gold helix photonic metamaterial as broadband circular polarizer. *Science* **325**, 1513 (2009).
12. Zhao, Y., Belkin, M. A. & Alù, A. Twisted optical metamaterials for planarized ultrathin broadband circular polarizers. *Nat. Commun.* **3**, 870 (2012).
13. Cui, Y., Kang, L., Lan, S., Rodrigues, S. & Cai, W. Giant chiral optical response from a twisted-arc metamaterial. *Nano Lett.* **14**, 1021–1025 (2014).
14. Yan, B. *et al*. Planar chiral metamaterial design utilizing metal-silicides for giant circular dichroism and polarization rotation in the infrared region. *Opt. Commun.* **383**, 57–63 (2017).
15. De Leon, I. *et al*. Strong, spectrally-tunable chirality in diffractive metasurfaces. *Sci. Rep.* **5**, 13034 (2015).
16. Li, W. *et al*. Circularly polarized light detection with hot electrons in chiral plasmonic metamaterials. *Nat. Commun.* **6**, 8379 (2015).
17. Li, Z., Liu, W., Cheng, H., Chen, S. & Tian, J. Tunable dual-band asymmetric transmission for circularly polarized waves with graphene planar chiral metasurfaces. *Opt. Lett.* **41**, 3142–3145 (2016).
18. Rodrigues, S. P., Cui, Y., Lan, S., Kang, L. & Cai, W. Metamaterials Enable Chiral-Selective Enhancement of Two-Photon Luminescence from Quantum Emitters. *Adv. Mater.* **27**, 1124–1130 (2015).
19. Wang, Z. *et al*. Circular dichroism metamirrors with near-perfect extinction. *ACS Photonics* **3**, 2096–2101 (2016).
20. Kenney, M. *et al*. Pancharatnam-Berry Phase Induced Spin-Selective Transmission in Herringbone Dielectric Metamaterials. *Adv. Mater.* **28**, 9567–9572 (2016).
21. Menzel, C., Carsten, R. & Falk, L. Advanced Jones calculus for the classification of periodic metamaterials. *Phys. Rev. A* **82**, 053811 (2010).
22. Ma, S. *et al*. Ultra-wide band reflective metamaterial wave plates for terahertz waves. *EPL* **117**, 37007 (2017).
23. Zhao, Y., Shi, J., Sun, L., Li, X. & Alù, A. Alignment-Free Three-Dimensional Optical Metamaterials. *Adv. Mater.* **26**, 1439–1445 (2014).
24. Luo, W., Xiao, S., He, Q., Sun, S. & Zhou, L. Photonic spin Hall effect with nearly 100% efficiency. *Adv. Opt. Mater.* **3**, 1102–1108 (2015).
25. Alaeian, H. & Dionne, J. A. Controlling electric, magnetic, and chiral dipolar emission with PT-symmetric potentials. *Phys. Rev. B* **91**, 245108 (2015).
26. Wang, Z. *et al*. Origami-Based Reconfigurable Metamaterials for Tunable Chirality *Adv. Mater*. doi:10.1002/adma.201700412.
27. Ordal, M. A. *et al*. Optical properties of the metals Al, Co, Cu, Au, Fe, Pb, Ni, Pd, Pt, Ag, Ti, and W in the infrared and far infrared. *Appl. Opt.* **22**, 1099 (1983).
28. Zhang, S. *et al*. Demonstration of metal-dielectric negative-index metamaterials with improved performance at optical frequencies. *J. Opt. Soc. Am. B* **23**, 434–438 (2006).

Acknowledgements

This work was supported by the National Key Research and Development Program of China (2016YFA0301102), the Natural Science Foundation of China (11574163 and 61378006), and the Program for New Century Excellent Talents in University (NCET-13-0294). We also acknowledge the support from the Collaborative Innovation Center of Extreme Optics, Shan xi University, Taiyuan, Shanxi 030006, China.

Author Contributions

Z.L. and S.C. designed the metasurface and developed the theory analysis. Z.L. together with W.L., H.C. and S.C. performed the simulation results. Z.L., S.C. and J.T. co-wrote the paper. All the authors discussed the results and commented on the manuscript.

Additional Information

Competing Interests: The authors declare that they have no competing interests.

Publisher's note: Springer Nature remains neutral with regard to jurisdictional claims in published maps and institutional affiliations.

Open Access This article is licensed under a Creative Commons Attribution 4.0 International License, which permits use, sharing, adaptation, distribution and reproduction in any medium or format, as long as you give appropriate credit to the original author(s) and the source, provide a link to the Creative Commons license, and indicate if changes were made. The images or other third party material in this article are included in the article's Creative Commons license, unless indicated otherwise in a credit line to the material. If material is not included in the article's Creative Commons license and your intended use is not permitted by statutory regulation or exceeds the permitted use, you will need to obtain permission directly from the copyright holder. To view a copy of this license, visit http://creativecommons.org/licenses/by/4.0/.

© The Author(s) 2017